



A cascaded control strategy for magneto-rheological dampers based on Hammerstein model

Shuyou Yu ^{a,b}, Jie Guo ^a, Xinze Xu ^a, Songlin Zhang ^a, Baojun Lin ^{a,*}

^a Department of Control Science and Engineering, Jilin University, Changchun 130012, China

^b Key Laboratory of Industrial Internet of Things and Networked Control, Chongqing University of Posts and Telecommunications, Chongqing, 400065, China

ARTICLE INFO

Communicated by X. Jing

Keywords:

Magneto-rheological damper
Hammerstein model
Cascaded control
Seat suspension

ABSTRACT

In order to effectively attenuate the inherent hysteresis nonlinearity of magneto-rheological (MR) dampers, and achieve precise tracking control of damping force, a cascaded control strategy based on Hammerstein model is proposed in this paper. A BP neural network is utilized to construct the nonlinear module of Hammerstein model, which accurately captures the hysteresis behavior of MR dampers. The dynamic characteristics of the dampers are then described by a linear time-invariant model. For MR dampers, the cascaded control strategy enhances the robustness of the system compared to traditional open-loop control based on the inverse model schemes. The effectiveness of the proposed control algorithm has been verified through simulation experiments and hardware-in-the-loop experiments using a seat suspension testbed equipped with MR dampers.

1. Introduction

Magneto-rheological (MR) fluid is an intelligent material that is extensively utilized in various industries. This is mainly due to its ability to exhibit instantaneous reversible rheological behavior in the presence of a magnetic field, and the consistent relationship between yield stress and magnetic field intensity [1]. MR dampers, which utilize MR fluid, have proven to be effective in reducing vibrations caused by road disturbances, thereby improving ride comfort and handling comfort [2]. However, the hysteresis characteristics of MR dampers can result in complex nonlinear dynamic behavior [3]. To attenuate the hysteresis effect and achieve better vibration isolation performance, appropriate modeling methods and control strategies need to be employed [4].

Various models have been developed to describe the nonlinear dynamic characteristics of MR dampers, which can be broadly classified into parametric models (Bingham model, Bouc-Wen model, and so on) [5,6] and nonparametric models (especially neural network models) [7,8].

The most classical control method for seat suspension systems equipped with MR dampers is hierarchical control [9]. The upper level uses control strategies such as sliding mode control to calculate the desired damping force for the seat suspension, while the lower level uses an open-loop control based on the inverse model (OLC-IM) to obtain the desired control current for the MR damper [10,11]. However, the lower level open-loop control method cannot actively compensate for disturbances or perturbations in the system. For example, the MR fluid exhibits different characteristics with temperature changes, i.e., with increasing temperature, the MR fluid tends to expand, thereby reducing its yield stress. Conversely, at low temperatures, the viscosity stress of the MR fluid increases, leading to a more pronounced decrease in its shear damping capability [12]. In practical applications, dissipated power

* Corresponding author.

E-mail address: linbj@jlu.edu.cn (B. Lin).

<https://doi.org/10.1016/j.ymssp.2024.111748>

Received 27 April 2024; Received in revised form 2 July 2024; Accepted 16 July 2024

0888-3270/© 2024 The Authors. Published by Elsevier Ltd. This is an open access article under the CC BY-NC-ND license (<http://creativecommons.org/licenses/by-nc-nd/4.0/>).

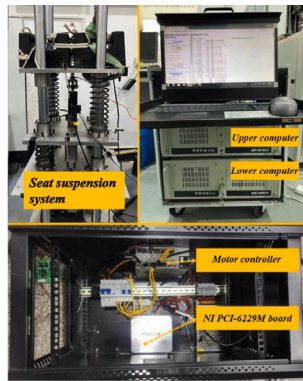


Fig. 1. The testbed used for Experiments.

is converted into internal energy, causing an increase in temperature, altering the performance of the MR fluid, and significantly reducing the damping force. The model-plant mismatches hinder precise force control of the MR damper [13]. Therefore, for a seat suspension system equipped with MR dampers, the controller needs to be robust to temperature changes, changes in MR fluid performance, and other system parameter variations, in order to maintain the desired damping force output. To address this issue, the Hammerstein-Wiener model which considers the impact of temperature during the modeling process, is proposed in [14,15]. The utilization of support vector machines for temperature modeling is discussed in [16]. The influence of temperature, and both the forward and inverse models are discussed in [17,18]. An inverse model is adopted to compensate for the influence of temperature [19]. The methods discussed earlier take into account the impact of temperature on damping force. However, to obtain an exact inverse model that accurately represents the relationship between temperature and damping force can be a challenging task. Furthermore, considering only the influence of temperature may not be sufficient to address the challenges brought by variations in other parameters. An integrated control method for semi-active suspension equipped with MR dampers is proposed in [20], which utilizes an H_∞ controller. However, this approach requires linearizing the complex nonlinear characteristics of the MR damper. A Fractional-order integrated sliding mode controller is provided for MR semi-active suspension in [21], but sliding mode control cannot directly handle system constraints. A fuzzy controller is designed in [22] for an MR semi-active suspension. However, the fuzzy approximation technique requires a significant amount of reliable prior knowledge.

From the above discussions, this paper adopts a hierarchical control strategy for seat suspension system equipped with MR dampers. For the lower level, a cascaded control strategy for MR dampers based on Hammerstein model is proposed. Hammerstein model offers a formal separation of the nonlinear and linear characteristics of the system, which is beneficial for system analysis and the design of cascaded control strategy. A static inverse model is to compensate for the nonlinear characteristic of the system in series in front of Hammerstein model. Subsequently, a triple-step controller is designed based on the model after inverse compensation to track the desired damping force calculated by upper level control scheme. Compared with the open-loop control for lower level, it can eliminate the influence of disturbances or perturbations and improve control accuracy. In contrast to integrated control, hierarchical control allows each level to be independently designed and optimized, improving control precision. Finally, the results of the simulation experiments demonstrate the robustness of the cascaded control strategy. It successfully achieves accurate tracking of the desired damping force, even in the presence of various disturbances. Furthermore, the hardware-in-the-loop experiments validated the practical feasibility and real-world applicability of the proposed control algorithm for MR dampers in seat suspension systems.

The structure of this paper is as follows: In Section 2, Hammerstein model of MR dampers is established by experimental data. In Section 3, an inverse model and the triple-step controller of the MR damper are designed, respectively. In Section 4, the simulation experiment of force tracking of the MR damper is carried out in Matlab/Simulink environment to verify the effectiveness of the proposed control scheme. In Section 5, physical experiments are conducted to assess the capability of the force tracking control algorithm and evaluate the performance of the seat suspension. Finally, conclusions are drawn.

2. Modeling and identification

In this section, experiments are conducted for the modeling of MR dampers, with a primary focus on its damping characteristics for vibration reduction and hysteresis behavior.

2.1. Experimental setup

The experimental data used in this paper is of the input–output measurements from an MR damper of a seat suspension system, as shown in Fig. 1, which is equipped with a MR damper, an electric motor power system, a data acquisition and control system, and a seat suspension system with sensors.

Table 1
Input signal information.

Frequency/(Hz)	Amplitude/(mm)	Maximum speed of piston motion/(m/s)
0.16	20	0.052
0.38	20	0.131
0.80	20 </td <td>0.262</td>	0.262
1.66	20	0.524

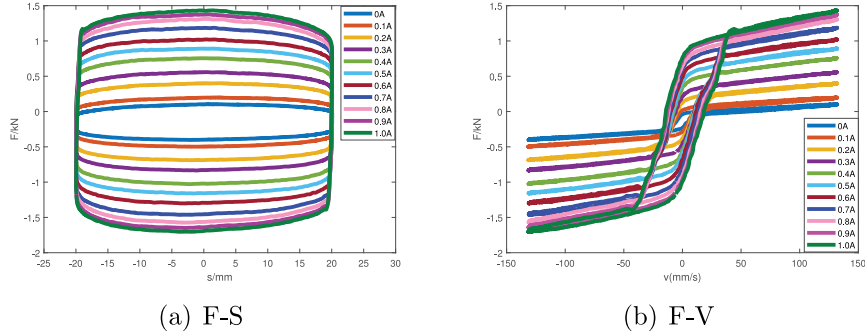


Fig. 2. Characteristic curves of MR damper at the maximum piston velocity $v = 0.131$ m/s.

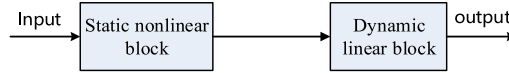


Fig. 3. The Hammerstein model structure.

Note that the motor utilized in the experimental setup has a rated power of 400 W, a stroke length of 200 mm, a rated output of 5.8 kN, and a maximum instantaneous output of 17.4 kN. This motor is responsible for generating the actuating force required by the experimental system.

The hardware of the data acquisition and control system primarily consists of an upper and a lower industrial computers, data acquisition cards, and current drive boards. The board card installed in the industrial computer has 32 analog input ports, 4 analog output ports, and 48 digital input/output ports, which facilitate the acquisition and control of data in the experimental system. For the MR damper, the control current is supplied by a current drive board, which operates on an 18–24 V voltage range. The drive board is capable of generating a control current proportional to the input voltage, with a maximum output current of 2 A. By sending a voltage signal to the drive board, effective damping control can be achieved.

To measure the acceleration of the seat suspension, two ADXL202 acceleration measurement modules are used. Additionally, a draw-wire encoder, BRT38-4M/5M, is utilized to measure the relative displacement of the piston rod. A force sensor, RDF-8, is employed to measure the force generated by the MR damper.

According to the standard QC/T545-1999 “Test Methods for Vehicle Cylinder Dampers on the testbed”, the input signals for the external characteristic testing of MR dampers include piston stroke, piston velocity, and control current. The piston stroke is selected as sinusoidal signals with frequencies of 0.16 Hz, 0.38 Hz, 0.80 Hz, and 1.66 Hz, respectively. The corresponding maximum piston velocities for the four groups are 0.052 m/s, 0.131 m/s, 0.262 m/s, and 0.524 m/s, respectively, as shown in Table 1. The vertical direction test is conducted, where the initial position of the piston rod is tuned to the middle of the damper. Different values of current ranging from 0 A to 1.0 A in increments of 0.1 A are applied during the test.

For brevity, only the responses of the MR damper at a frequency of 0.38 Hz and a maximum piston velocity of 0.131 m/s are shown in Fig. 2. The Force-Stroke (F-S) curve in Fig. 2(a) demonstrates that the MR damper exhibits excellent energy dissipation characteristics. The Force-Velocity (F-V) curve in Fig. 2(b) highlights the significant hysteresis of the MR damper. Additionally, as the input current increases, the damping force markedly rises [23].

The experimental data needs to be normalized, i.e., the experimental data is converted into the set of (0, 1). In this paper, the neural network is trained with 75% of the experimental data, and the accuracy of the trained neural network model is tested with the rest of 25% of the experimental data.

2.2. Establishment of Hammerstein model

Considering the strong nonlinearity and hysteresis characteristics of MR dampers, a Hammerstein model is established, which offers significant advantages for system analysis and the design of cascaded control strategy. The structure is shown in Fig. 3.

(1) Static nonlinear block

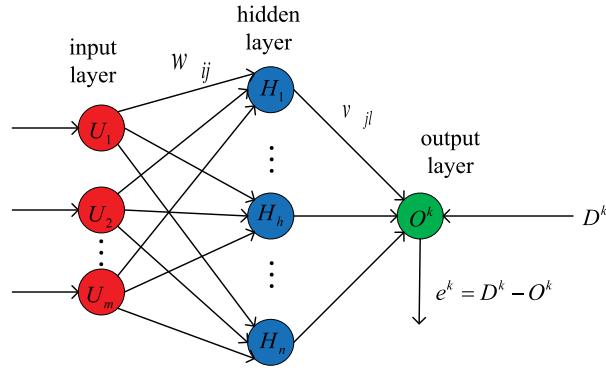


Fig. 4. The structure of the BP neural network. $U_{1,2,\dots,m}$: the input signal. $H_{1,2,\dots,n}$: the output of the hidden layer. O^k : the output of the neural network. D^k : actual output. w_{ij} and v_{jl} : weight values of different layers.

The static nonlinear block is responsible for describing the main force contribution. To accurately capture the complex nonlinear behavior exhibited by MR dampers, a BP neural network is used to approximate the static nonlinear block, which is shown in Fig. 4.

The design of the BP neural network is as follows:

(1) Parameter determination

Due to the hysteresis characteristic of the MR damper, the output of its network depends not only on the current input but also on past inputs and outputs.

Hence, this paper proposes a special structure of the BP neural network that incorporates the output of the damping force from the previous moment as an input to improve modeling accuracy, as shown in Fig. 4.

Therefore, the number m of nodes of the input layer is 4, which are the current, piston displacement, piston velocity, and the output of the damping force at the previous moment, respectively. The damping force is the only output of the output layer.

The number of neurons in the hidden layer (q) is designed according to the empirical formula $q = \sqrt{m+g} + a$, where m/g represents the number of neurons in the input/output layer of the BP neural network, respectively. The term a is a constant from 1 to 10. The final value of the number of neurons in the hidden layer is determined as 12 by trial-and-error method [24].

(2) The training function

The excitation functions of neurons of hidden layer and output layer adopt hyperbolic tangent sigmoid function and linear function respectively, which makes it possible to approximate an arbitrary nonlinearity between inputs and outputs. The mean square error (MSE) between the actual output (D^k) and the output of the neural network (O^k) is chosen as the performance function, and the Levenberg–Marquardt algorithm is used as the training function of the BP neural network [25].

(2) Dynamic linear block

BP neural network is essentially a static nonlinear mapping. In order to reduce the approximation error, dynamic characteristics are introduced. The damping force generated by the static nonlinear block is taken as the input, and the actual damping force is treated as the output. The order of numerator and denominator of the dynamic linear system is determined by trial-and-error, and the parameters are identified by the least square method. Finally, a transfer function is determined as follows

$$G(s) = \frac{579800}{s^2 + 671.5s + 579900} \tag{1}$$

The transfer function (1) is stable because both its poles are located in the left half-plane of the virtual axis, and there is no zero point.

A state space equation of the transfer function is shown as follows

$$\begin{bmatrix} \dot{x}_1 \\ \dot{x}_2 \end{bmatrix} = \begin{bmatrix} 0 & 1 \\ -579900 & -671.5 \end{bmatrix} \begin{bmatrix} x_1 \\ x_2 \end{bmatrix} + \begin{bmatrix} 0 \\ 1 \end{bmatrix} u$$

$$y = \begin{bmatrix} 579800 & 0 \end{bmatrix} \begin{bmatrix} x_1 \\ x_2 \end{bmatrix} \tag{2}$$

Remark 1. The terms of x_1 and x_2 in (2) have no physical meaning. The input variable of u is the damping force generated by the static nonlinear block, and the output variable of y is the “actual” damping force.

2.3. Model verification

(1) Results of the BP neural network model

The model is verified with the data of the excitation velocity of 0.131 m/s, the amplitude of 20 mm, the MSEs of the training and test data have reached 10^{-4} . Curves of both the force-piston displacement and force-piston velocity are shown in Fig. 5. From

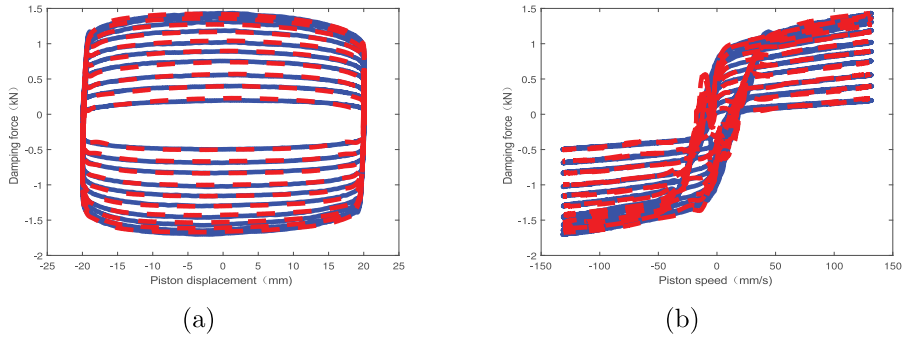


Fig. 5. Results of the BP neural network model. Blue solid lines: experimental data. Red dotted lines: the BP neural network model output.

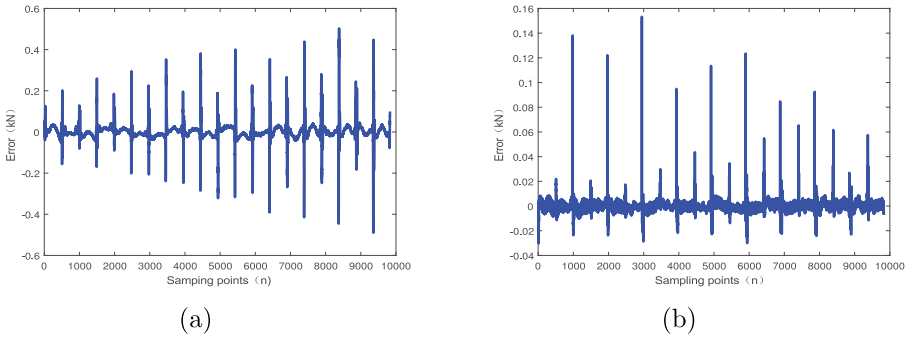


Fig. 6. Comparison of modeling error. (a): Without damping force at previous moment. (b): With damping force at previous moment.

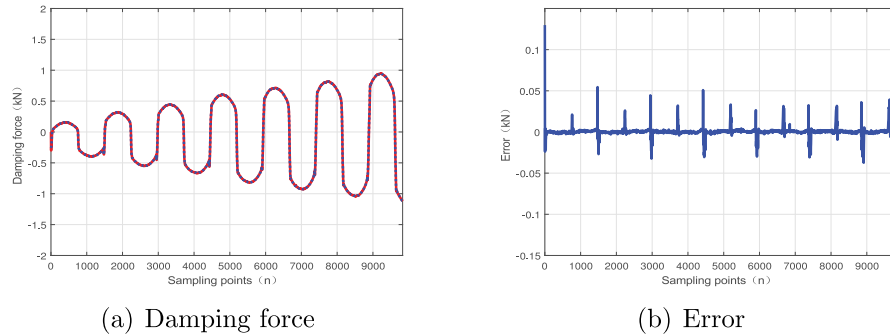


Fig. 7. Comparison of damping force generated by the Hammerstein model and actual damping force. Red solid line: actual damping force. Blue dotted line: Hammerstein model damping force.

Fig. 5(b), it can be observed that there exists slight deviation between the predicted curve and the experimental curve, in particular, in the hysteresis cycle.

From Fig. 6, it reveals that by using the previous output damping force as input, the nonlinearity and hysteresis characteristic of the MR damper can be better described, and resulting in improved tracking accuracy.

(2) Results of Hammerstein model

Data of different current values with the piston velocity of 0.131 m/s and amplitude of 20 mm are selected to verify the effectiveness of the obtained Hammerstein model. The damping force generated by the model and the actual damping force are shown in Fig. 7(a). From Fig. 7(b), it demonstrates that the maximum error is 0.05 kN, and the MSE of them is less than 0.000042. Note that, compared with the static nonlinear block, the maximum error is much smaller.

3. Controller design

This section focuses on the controller design problem of the MR damper, aiming to improve its force tracking performance and enhance the overall performance of the vehicle seat in terms of vertical dynamics.

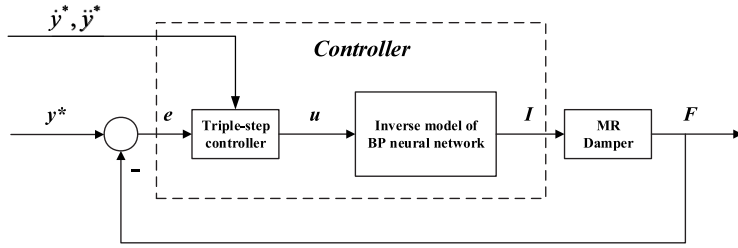


Fig. 8. Block diagram of MR damper control system structure.

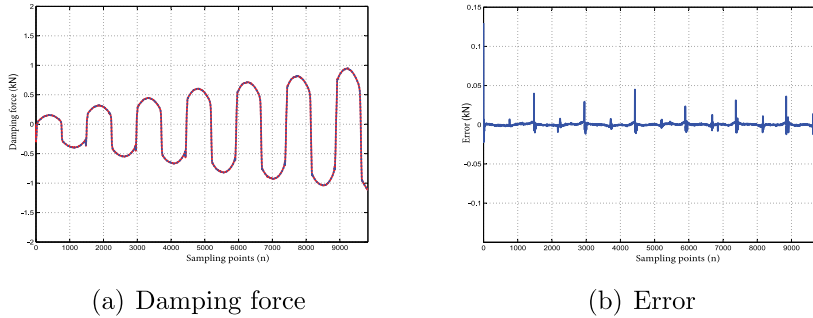


Fig. 9. Comparison of tracking diagram of damping force after inverse model compensation. Red solid line: actual damping force. Blue dotted line: Hammerstein model damping force.

A hierarchical control strategy is adopted, with a cascaded control method employed at the lower level to ensure the MR damper can track the desired damping force quickly and accurately. The control structure is shown in Fig. 8, which includes a triple-step controller module, an inverse model module, and the controlled MR damper. The term of y^* represents the desired damping force calculated by the upper level controller. It should be noted that the control current I generated by the inverse model is used to control the MR damper.

3.1. An inverse model of the MR damper

The accuracy of the force-to-voltage/current mapping determines the tracking performance of the damping force. However, for the OLC-IM, the potential model-plant mismatches that may arise from temperature changes, changes in MR fluid performance, and other variations in system parameters are disregarded.

In this paper, the proposed cascaded control strategy is composed of an inverse model and a triple-step controller in series. The inverse model is connected in series with Hammerstein model to compensate for its nonlinear part [26], and a BP neural network is selected to train the inverse model.

The relative displacement, velocity, and damping force of the piston rod at this moment and the current value at the previous moment are chosen as the inputs. The current at present is chosen as the output. Specific steps are the same as the static nonlinear block mentioned earlier, and will not be repeated here.

Figs. 9(a) and 9(b) illustrate that Hammerstein model in series with the inverse model exhibits satisfactory tracking performance, but there are still noticeable errors between the actual output and the model output. These errors need to be attenuated to minimize their impact on the system dynamics.

3.2. Triple-step controller

A triple-step controller is designed for the linear model of Hammerstein model after the inverse compensation, taking the compensation errors and model uncertainties as disturbances. The triple-step controller includes a steady-state-like control module, a reference-dynamic-based feedforward control module, and an error feedback control module [27], which structure is shown in the dashed box of Fig. 10.

Step 1: Steady-state-like control

The state space model (2) is expressed as follows:

$$\begin{aligned} \dot{x}_1 &= x_2 \\ \dot{x}_2 &= ax_1 + bx_2 + u \\ y &= cx_1 \end{aligned} \tag{3}$$

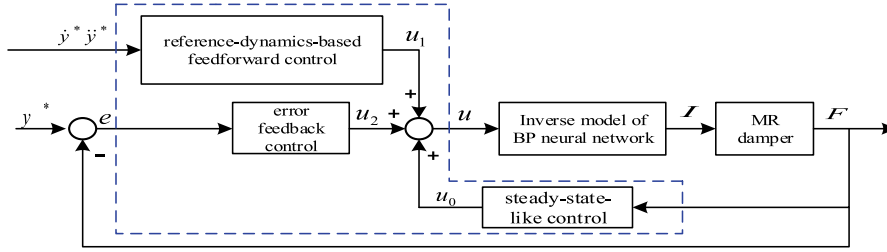


Fig. 10. Control structure of a MR damper with triple-step controller.

with $a = -579900$, $b = -671.5$, $c = 579800$.

Suppose that the system has reached a steady state, i.e., $\dot{y} = 0$, $\ddot{y} = 0$, then

$$0 = \dot{y} = c\dot{x}_1 = cx_2 \quad (4)$$

$$0 = \ddot{y} = c\dot{x}_2 = c(ax_1 + bx_2 + u) \quad (5)$$

By enforcing $u = u_0$, then the steady-state-like control law can be obtained as follows:

$$u_0 = -ax_1 \quad (6)$$

Step 2: Reference-dynamics-based feedforward control

Define the reference signal as y^* , which might change with working conditions of the system. In order to improve characteristics of the system, the changes of the reference signal are taken into consideration, i.e., a reference-dynamic-based feedforward control law is designed. Then, the control law becomes:

$$u = u_0 + u_1 \quad (7)$$

Substituting (7) into (5), one has

$$\ddot{y} = bx_2 + u_1 \quad (8)$$

Then, by enforcing $\ddot{y} = \ddot{y}^*$, the reference-dynamics-based feedforward control law is

$$u_1 = \ddot{y}^* - bx_2 \quad (9)$$

Step 3: Error feedback control

Due to high-order unmodeled dynamics of system or external disturbances, systems with the control law derived from the first two steps often have a certain tracking deviation. Error feedback control introduced can further reduce the tracking deviation, and improve the robustness to uncertainties.

Define the tracking error of the system as $e_1 = y^* - y$. Suppose the feedback control to be determined is u_2 , then the controller of the system becomes:

$$u = u_0 + u_1 + u_2 \quad (10)$$

Substituting (10) into (5), one has

$$\ddot{y} = \ddot{y}^* + u_2 \quad (11)$$

The first derivative and second derivative with respect to time of the system tracking error e_1 are:

$$\dot{e}_1 = \dot{y}^* - \dot{y} \quad (12)$$

$$\ddot{e}_1 = \ddot{y}^* - \ddot{y} = -u_2 \quad (13)$$

By enforcing $e_2 = \dot{e}_1$, (13) is

$$\dot{e}_2 = \ddot{e}_1 = -u_2 \quad (14)$$

Construct a candidate Lyapunov function:

$$V_1 = \frac{1}{2}e_1^2 + \frac{1}{2}k_0\chi^2 \quad (15)$$

where $k_0 > 0$, and $\chi = \int e_1 dt$. The derivative of V_1 with respect to time is

$$\begin{aligned} \dot{V}_1 &= e_1\dot{e}_1 + k_0e_1\chi \\ &= e_1e_2 + k_0e_1\chi \end{aligned} \quad (16)$$

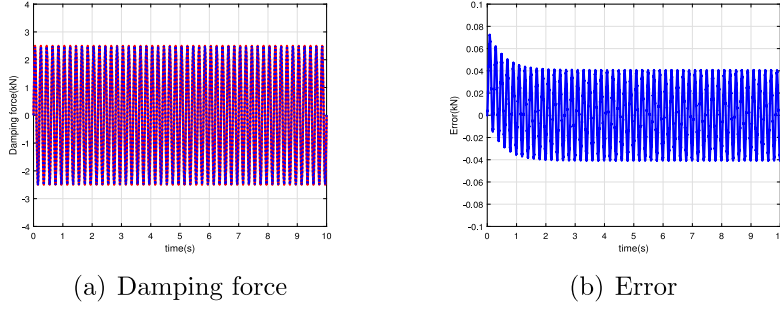


Fig. 11. Curves of the desired force tracking and error ($f = 5$ Hz). Red solid line: desired damping force, blue dotted line: output damping force by cascaded control, blue solid line: tracking error. (For interpretation of the references to color in this figure legend, the reader is referred to the web version of this article.)

In order to force the error system asymptotically stable, select the virtual control variable $e_2^* = -k_1 e_1 - k_0 \chi$, where $k_1 > 0$. By enforcing $e_2 = e_2^*$, then

$$\dot{V}_1 = -k_1 e_1^2 \quad (17)$$

$$\dot{e}_1 = -k_1 e_1 - k_0 \chi \quad (18)$$

Note that in the system process, in general, $e_2 \neq e_2^*$. Denote $e_3 = e_2^* - e_2$. Then, (17) and (18) become

$$\dot{V}_1 = -k_1 e_1^2 - e_1 e_3 \quad (19)$$

$$\dot{e}_1 = -k_1 e_1 - k_0 \chi - e_3 \quad (20)$$

From (14) and $e_2^* = -k_1 e_1 - k_0 \chi$, $e_2 = \dot{e}_1$, one has

$$\begin{aligned} \dot{e}_3 &= \dot{e}_2^* - \dot{e}_2 \\ &= -k_1 \dot{e}_1 - k_0 \dot{\chi} + u_2 \end{aligned} \quad (21)$$

By enforcing $V_2 = V_1 + \frac{1}{2} e_3^2$, then

$$\begin{aligned} \dot{V}_2 &= \dot{V}_1 + e_3 \dot{e}_3 \\ &= -k_1 e_1^2 + e_3 [u_2 - (k_0 + 1) e_1 - k_1 \dot{e}_1] \end{aligned} \quad (22)$$

In order to ensure the negative definite of V_2 , the control law is selected as

$$u_2 = k_1 \dot{e}_1 + (k_0 + 1) e_1 - k_2 e_3 \quad (23)$$

Combining $e_2^* = -k_1 e_1 - k_0 \chi$ and $e_2 = \dot{e}_1$, the control law is as follows

$$u_2 = (k_0 + 1 - k_1^2 + k_1 k_2) e_1 + k_0 (k_2 - k_1) \int e_1 dt + k_2 \dot{e}_1 \quad (24)$$

Combining (6) and (9), the final control law is

$$u = u_0 + u_1 + u_2 \quad (25)$$

Remark 2. The triple-step controller adopts the ‘feedforward and feedback’ control structure, which has strong robustness to disturbances or uncertainties. Note that steady-state-like control law mainly reflects the characteristic of the system, and the reference-dynamics-based feedforward control law provides a correction behavior while the reference of the system is changing.

4. Simulation analysis

In order to verify the effectiveness of the proposed control strategy, the simulation experiments of damping force tracking control are carried out. The steady-state-like control parameter a of the designed triple-step controller is -579900 , the reference-dynamics-based feedforward control parameter b is -671.5 , and the error feedback control parameters k_0, k_1, k_2 is $3994, 2496, 2000$ respectively. First, a tracking experiment is performed on a single frequency reference signal, i.e., $y^* = 2.5 \sin(2\pi f t)$ kN. The frequency f of the reference signal is selected as 5 Hz. The simulation results are in Fig. 11, which show that the MR damper can track the desired damping force accurately. In order to further verify the effectiveness of the designed controller, composite frequency signals are selected as $y^* = 1 - 2 \sin(2 - \cos(2\pi f_1 t) - \cos(2\pi f_2 t))$ kN, where the frequencies are set as $f_1 = 0.5$ Hz, $f_2 = 3$ Hz.

Fig. 12 shows that the designed controller is capable of maintaining the tracking performance of the system for the composite frequency signals.

Table 2 shows the maximum error, error percentage, and MSE of the MR damper. The values of the MSE are below the level of 10^{-4} , and the maximum error percentage is 3.1411%, which demonstrate the effectiveness of the proposed control strategy.

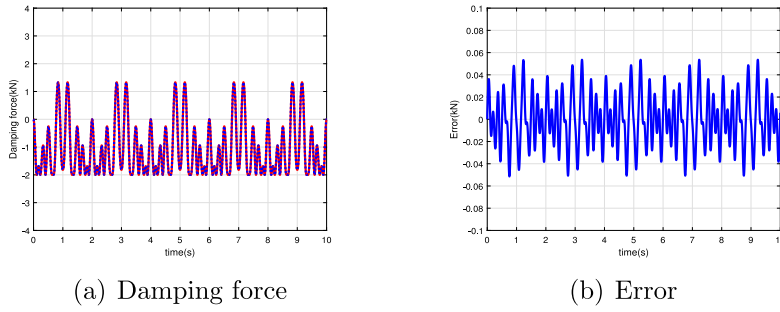


Fig. 12. Curves of the desired force tracking and error ($f = (0.5,3)$ Hz). Red solid line: desired damping force, blue dotted line: output damping force by cascaded control, blue solid line: tracking error. (For interpretation of the references to color in this figure legend, the reader is referred to the web version of this article.)

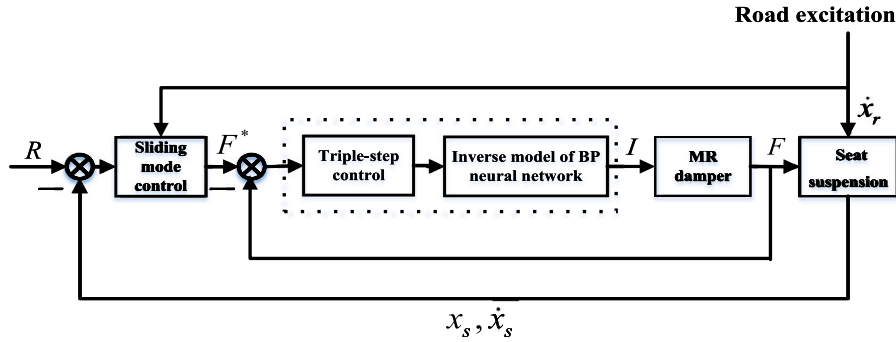


Fig. 13. Block diagram of semi-active seat suspension equipped with MR damper.

Table 2

Maximum tracking error, error percentage, mean square error with different frequency signals.

Signal frequency	Max error/kN	Percentage/%	MSE/kN
5 Hz	0.0725	2.8995	8.5024×10^{-4}
(0.5,3) Hz	0.0536	2.1422	5.7273×10^{-4}

5. Experiment

In this section, the proposed control strategy has been applied to a semi-active seat suspension equipped with MR dampers [28]. A hierarchical control strategy is adopted, which is shown in Fig. 13. In the upper level, the seat suspension utilizes a sliding mode controller based on barrier functions [29] to calculate the desired damping force F^* . x_s and \dot{x}_s represent the velocity and displacement of the sprung mass, respectively.

In the lower level, experiments on damping force tracking control and suspension performance testing are conducted under various road conditions. Additionally, temperature rise can be used as an example to validate the robustness of the cascaded control strategy in the presence of model-plant mismatches.

Remark 3. In the experiment section, the maximum piston velocity of the damper is set to 0.131 m/s. As shown in Fig. 2, the output damping force of the MR damper ranges from -1500 N to 1500 N. Therefore, for the upper-level control, we use barrier functions to limit the maximum damping force within $[-1500$ N, 1500 N]. Consequently, the obtained current varies within the range of $[0$ A, 1 A].

(1) Damping force tracking on various road surfaces with MR dampers at room temperature conditions

Experiments of the damping force tracking performance with MR dampers at room temperature conditions are conducted on a sinusoidal road surface with a frequency of 2.5 Hz and an amplitude of 0.05 m, which are shown in Fig. 14(a). It is identified that the proposed cascaded control strategy is more effective in tracking the desired damping force compared to the OLC-IM.

The experimental results, depicted in Fig. 14(b), validate the effectiveness of the proposed control strategy on a randomly rough Class C road pavement.

Table 3
Experimental results of triple-step method.

Road surface	Max error/kN	MSE/(kN) ²
Sinusoidal	0.1331	2.6284×10^{-3}
Random	0.1288	2.7764×10^{-3}

Table 4
Experimental results of the OLC-IM.

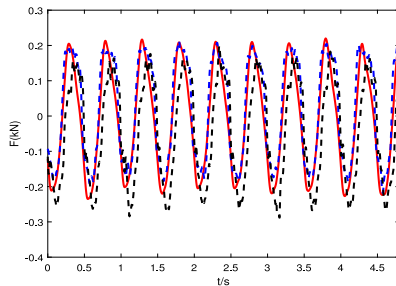
Road surface	Max error/kN	MSE/(kN) ²
Sinusoidal	0.2112	8.1997×10^{-3}
Random	0.2262	8.2591×10^{-3}

Table 5
Experimental results of triple-step method control at high temperature conditions.

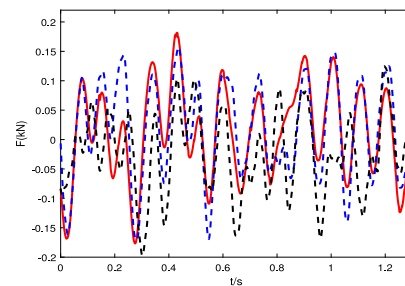
Road surface	Max error/kN	MSE/(kN) ²
Sinusoidal	0.1248	2.7633×10^{-3}
Random	0.1772	3.6731×10^{-3}

Table 6
Experimental results of the OLC-IM at high temperature conditions.

Road surface	Max error/kN	MSE/(kN) ²
Sinusoidal	0.2944	2.1997×10^{-2}
Random	0.2740	1.2313×10^{-2}



(a) Sinusoidal road surface



(b) Random road surface

Fig. 14. Curves of the desired force tracking with MR dampers at room temperature conditions. Red solid line: desired damping force, blue dotted line: output damping force by cascaded control, black dotted line: output damping force by the OLC-IM. (For interpretation of the references to color in this figure legend, the reader is referred to the web version of this article.)

Tables 3–4 present the maximum error and MSE of the results obtained from the damping force tracking experiments using the two aforementioned methods, it can be concluded that both the proposed control strategy and the OLC-IM can achieve satisfying tracking performance of the damping force, and the proposed control strategy exhibits slightly better performance.

(2) The robustness of cascaded control for MR dampers at high temperature conditions

The OLC-IM is commonly used in the control of MR dampers. However, this method faces challenges in dealing with disturbances and perturbations, particularly due to the temperature sensitivity and sedimentation characteristics of MR fluids [30]. Since there is no temperature sensors of the MR damper on the testbed, the precise temperature of the MR damper could not be accurately measured. According to [30], continuously applying the maximum current permitted by the testbed, 1 A, to the MR damper for 3 min, the fluid temperature rises significantly, and the damping characteristics of the actual system will be altered. (At this point, the temperature rise is noticeably felt by touch.) Notably, the proposed cascaded control strategy does not require to know the exact temperature value. The experimental results, shown in Fig. 15, provide valuable insights into the performance of the cascaded control strategy.

It can be concluded that while the damping characteristics of the actual system are altered by temperature changes, leading to model-plant mismatches, the OLC-IM cannot track the desired force anymore. In contrast, the proposed control strategy is still capable of effectively tracking the desired damping force.

The results of the maximum error and MSE of damping force tracking experiments with the heated MR damper using the above two methods are shown in Tables 5–6.

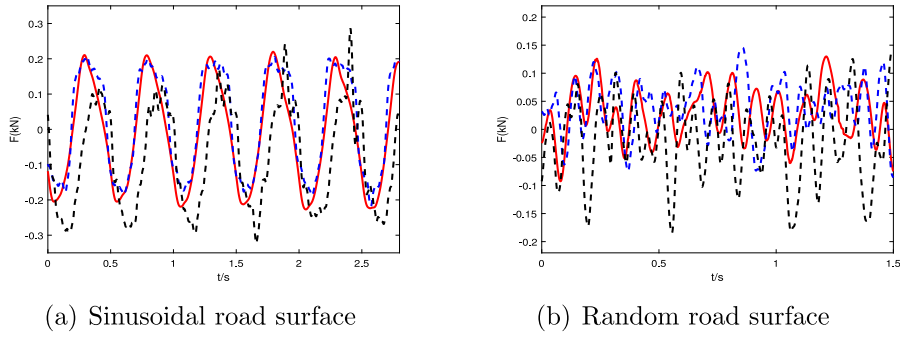


Fig. 15. Curves of the desired force tracking with MR dampers at high temperature conditions. Red solid line: desired damping force, blue dotted line: output damping force by cascaded control, black dotted line: output damping force by the OLC-IM. (For interpretation of the references to color in this figure legend, the reader is referred to the web version of this article.)

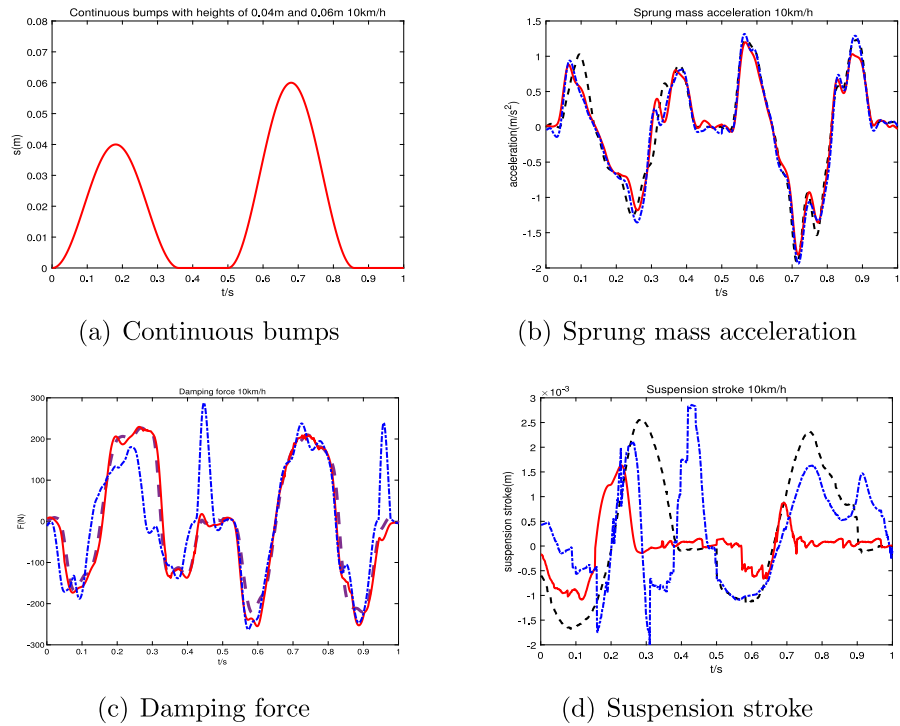


Fig. 16. Time-domain response of the seat suspension at a speed of 10 km/h. Red solid line: cascaded control, blue dotted line: the OLC-IM, black dashed line in (b) and (d): passive suspension, purple dotted line in (c): desired damping force. (For interpretation of the references to color in this figure legend, the reader is referred to the web version of this article.)

The above experimental results indicate that the OLC-IM leads to a significant reduction in tracking accuracy while the MR damper heats up. However, the proposed control strategy can effectively attenuate model mismatch of the inverse model and achieve satisfactory tracking performance with MSEs less than 10^{-3} .

(3) Performance evaluation of seat suspension with an MR damper

The robustness of the proposed control strategy is evaluated on a continuous bump road surface with an MR damper at high temperature conditions. The performance of the seat suspension system is shown in Figs. 16–17.

At a speed of 10 km/h, passing through continuous bumps with heights of 0.04 m and 0.06 m, time-domain response of the seat suspension system is depicted in Fig. 16. Fig. 16(b) displays the vertical acceleration of the seat, and it can be observed that the proposed control strategy performs slightly better than the other two methods. Fig. 16(c) illustrates the damping force curve, indicating temperature-induced model-plant mismatches at 0.45 s and 0.95 s. The force tracking performance of the OLC-IM is poor, resulting in significant fluctuations in the suspension stroke, as shown in Fig. 16(d). Compared to the OLC-IM, the proposed cascaded control strategy can effectively track the desired damping force, ensuring the ride comfort of the seat suspension system.

When the vehicle speed increases to 30 km/h, the time-domain response of the seat suspension system is shown in Fig. 17.

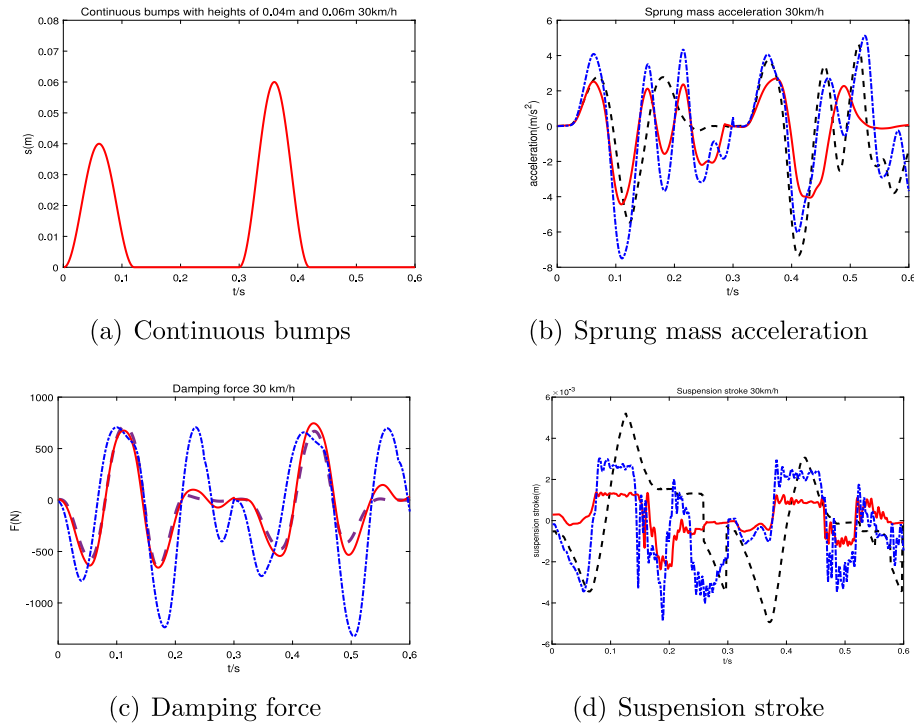


Fig. 17. Time-domain response of the seat suspension at a speed of 30 km/h. Red solid line: cascaded control, blue dotted line: the OLC-IM, black dashed line in (b) and (d): passive suspension, purple dotted line in (c): desired damping force. (For interpretation of the references to color in this figure legend, the reader is referred to the web version of this article.)

The OLC-IM has lost its ability to track the damping force, resulting in inferior ride comfort compared to passive control. However, the proposed cascaded control strategy can still ensure force tracking performance and exhibits significant advantages in terms of ride comfort.

In summary, the presence of temperature changes, variations in MR fluid performance, and other system parameter variations may lead to model-plant mismatches and a loss of damping force tracking performance for the OLC-IM schemes. However, the evaluation conducted on a testbed with an MR damper under temperature rises confirmed the robustness of the proposed control strategy in enhancing seat suspension performance under realistic operating conditions.

6. Conclusion

MR damper has strong nonlinearity and hysteresis characteristics. In this paper, a Hammerstein model that captures the nonlinear behavior of the MR fluid and the linear dynamics of the damper was established, providing a comprehensive representation of the system, as well as realizing a balance between accuracy and complexity. A cascaded control strategy was proposed to track the reference signal, attenuate unmodeled dynamics, and compensate for static errors. Experiments on a seat suspension with MR dampers traveling on a bump road were carried out to further evaluate the effectiveness of the proposed scheme. It showed the proposed scheme can improve tracking performance of the MR damper, and ride comfort of the seat suspension. Furthermore, it demonstrated as well that the proposed scheme is robust to model-plant mismatches, in particular, model-plant mismatches caused by temperature changes of the MR damper.

CRedit authorship contribution statement

Shuyou Yu: Supervision, Formal analysis. **Jie Guo:** Writing – review & editing, Writing – original draft, Software, Formal analysis. **Xinze Xu:** Software, Conceptualization. **Songlin Zhang:** Software. **Baojun Lin:** Writing – review & editing, Supervision, Investigation.

Declaration of competing interest

The authors declare that they have no conflicts of interest regarding the publication of this paper. No financial or personal relationships with other people or organizations that could influence the work have been disclosed. This research was conducted in an unbiased manner, adhering to ethical standards and scientific integrity.

Data availability

The data that has been used is confidential.

Acknowledgments

This work was supported in part by the National Natural Science Foundation of China under Grant No. U1964202, the Foundation of Key Laboratory of Industrial Internet of Things and Networked Control under Grant No. 2019FF01, the Natural Science Foundation of Jilin Province, China under Grant No. YDZJ202101ZYTS169.

References

- [1] Y. Hu, W. Xu, L. Qin, An axial flux permanent magnet motor with magneto-rheological fluid brake structure, *IEEE Trans. Magn.* 58 (8) (2022) 1–5.
- [2] P. Liu, D. Ning, L. Luo, et al., An electromagnetic variable inertia and damping seat suspension with controllable circuits, *IEEE Trans. Ind. Electron.* 69 (2022) 2811–2821.
- [3] H. Zhang, K. Cheng, E. Wang, et al., Nonlinear behaviors of a half-car magneto-rheological suspension system under harmonic road excitation, *IEEE Trans. Veh. Technol.* 72 (7) (2023) 8592–8600.
- [4] L. Yang, Z. Zhao, D. Li, Fractional order neural sliding mode control based on the FO-Hammerstein model of piezoelectric actuator, *ISA Trans.* (2023).
- [5] H. Lv, R. Chen, S. Zhang, Comparative experimental study on constitutive mechanical models of magnetorheological fluids, *Smart Mater. Struct.* (2018).
- [6] M. Versaci, A. Cutrupi, A. Palumbo, A magneto-thermo-static study of a magneto-rheological fluid damper: A finite element analysis, *IEEE Trans. Magn.* 57 (1) (2021) 1–10.
- [7] Z. Hou, Z. Feng, H. Hu, et al., Experimental study on performance characteristics of magnetorheological damper, *Adv. Eng. Des. Optim.* 37 (2011) 439–443.
- [8] S. Wei, J. Wang, J. Ou, Method for improving the neural network model of the magnetorheological damper, *Mech. Syst. Signal Process.* (2021).
- [9] D. Yoon, G. Kim, S. Choi, Response time of magnetorheological dampers to current inputs in a semi-active suspension system: Modeling, control and sensitivity analysis, *Mech. Syst. Signal Process.* 146 (2021).
- [10] Y. Hu, W. Gu, H. Zhang, et al., Adaptive robust triple-step control for compensating cogging torque and model uncertainty in a DC motor, *IEEE Trans. Syst. Man Cybern.* 49 (2019) 2396–2405.
- [11] G. Hu, L. Wu, Y. Deng, et al., Optimal design and performance analysis of magnetorheological damper based on multiphysics coupling model, *J. Magn. Magn. Mater.* 558 (2022).
- [12] A. Kariganaur, H. Kumar, M. Arun, Effect of temperature on sedimentation stability and flow characteristics of magnetorheological fluids with damper as the performance analyser, *J. Magn. Magn. Mater.* 555 (2022).
- [13] P.n Vishwakarma, P. Mishra, S. Sharma, Characterization of a magnetorheological fluid damper a review, *Mater. Today: Proc.* 56 (2022) 2988–2994.
- [14] G. Savaia, M. Corno, G. Panzani, et al., Temperature estimation in a magneto-rheological damper, in: *Proceedings of the 4th IEEE Conference on Control Technology and Applications*, 2020.
- [15] G. Savaia, G. Panzani, M. Corno, et al., Hammerstein-Wiener modelling of a magneto-rheological dampers considering the magnetization dynamics, *Control Eng. Pract.* (2021).
- [16] C. Priya, N. Gopalakrishnan, Temperature dependent modelling of magnetorheological(MR) dampers using support vector regression, *Smart Mater. Struct.* (2018).
- [17] J. Yu, X. Dong, X. Wang, et al., Asymmetric dynamic model of temperature-dependent magnetorheological damper and application for semi-active system, *Front. Mater.* (2019).
- [18] S. Jumani, An Invertible Open-Loop Nonlinear Dynamic Temperature Dependent MR Damper Model, Virginia Polytechnic Institute and State University, 2010.
- [19] G. Liang, T. Zhao, N. Li, et al., Magnetorheological damper temperature characteristics and control-oriented temperature-revised model, *Smart Mater. Struct.* 30 (2021).
- [20] J. Wu, H. Zhou, Z. Liu, et al., A load-dependent PWA H_∞ controller for semi-active suspensions to exploit the performance of MR dampers, *Mech. Syst. Signal Process.* 127 (2019) 441–462.
- [21] S. Nguyen, B. Lam, S. Choi, Smart dampers-based vibration control-Part 2: Fractional-order sliding control for vehicle suspension system, *Mech. Syst. Signal Process.* 148 (2021) 107145.
- [22] F. Meng, J. Zhou, Modeling and control of a shear-valve mode MR damper for semiactive vehicle suspension, *Math. Probl. Eng.* (2019).
- [23] J. Yang, D. Ning, S.S. Sun, et al., A semi-active suspension using a magnetorheological damper with nonlinear negative-stiffness component, *Mech. Syst. Signal Process.* 147 (2021).
- [24] Y. Sun, H. Chang, Z. Mia, Research on BP neural network model for water demand forecasting and its application, in: *2nd International Conference on Civil Engineering, Architecture and Building Materials*, 2012, pp. 170–173.
- [25] M. Haring, E.I. Grotli, S. Riemer-Sorensen, et al., A Levenberg–Marquardt algorithm for sparse identification of dynamical systems, *IEEE Trans. Neural Netw. Learn. Syst.* (2022).
- [26] A. Belabad, S. Sharifian, S. Motamedi, An accurate digital baseband predistorter design for linearization of RF power amplifiers by a genetic algorithm based Hammerstein structure, *Analog Integr. Circuits Signal Process.* 95 (2018) 231–247.
- [27] H. Chu, B. Gao, W. Gu, et al., Low speed control for permanent magnet DC torque motor using observer-based nonlinear triple-step controller, *IEEE Trans. Ind. Electron.* 64 (2017) 3286–3296.
- [28] W. Zhang, Study on Impedance Control of Commercial Vehicle Seat Suspension, Jilin University, 2023.
- [29] H. Obeid, L. Fridman, S. Laghrouche, et al., Barrier function-based adaptive integral sliding mode control, in: *2018 IEEE Conference on Decision and Control, CDC, Miami, FL, USA*, 2018, pp. 5946–5950.
- [30] A. Kariganaur, H. Kumar, M. Arun, Influence of temperature on magnetorheological fluid properties and damping performance, *Smart Mater. Struct.* 31 (2022).